Joint collaboration on comparing NOAA's ground-based weather radar and NASA-JAXA's spaceborne radar

Zhi Li,[a] Yixin Wen,[b] Liang Liao,[c] David Wolff,[d] Robert Meneghini,[e] Terry Schuur,[f,g]

[a] *School of Civil Engineering and Environmental Science, University of Oklahoma, Norman, Oklahoma, USA*

[b] *Department of Geography, University of Florida, Gainesville, Florida, USA*

[c] *NASA Goddard Earth Science Technology Research, Morgan State University, Baltimore, Maryland, USA*

[d] *NASA Wallops Flight Facility, Wallops Island, Virginia, USA*

[e] *NASA Goddard Space Flight Center, Greenbelt, Maryland, USA*

[f] *The Cooperative Institute for Severe and High-Impact Weather Research and Operations, University of Oklahoma, Norman, Oklahoma, USA*

[g] *NOAA/National Severe Storms Laboratory, Norman, Oklahoma, USA*

Corresponding author: Yixin Wen, yixin.wen@ufl.edu

Early Online Release: This preliminary version has been accepted for publication in *Bulletin of the American Meteorological Society*, may be fully cited, and has been assigned DOI 10.1175/BAMS-D-22-0127.1. The final typeset copyedited article will replace the EOR at the above DOI when it is published.

ABSTRACT

The National Aeronautics and Space Administration (NASA) and National Oceanic and Atmospheric Administration (NOAA) have a long and successful history of weather radar research. The NOAA ground-based radars – WSR-88D network – provide nationwide precipitation observations and estimates with advanced polarimetric capability. As a counterpart, the NASA-JAXA space-borne radar – the GPM/DPR (Global Precipitation Measurement Dual-frequency Precipitation Radar) – has global coverage and higher vertical resolution than ground-based radars. While significant advances from both NOAA's WSR-88D network and NASA-JAXA's spaceborne radar DPR have been made, no systematic comparisons between the WSR-88D network and the DPR have been done. This study for the first time generates nationwide comprehensive comparisons at 136 WSR-88D radar sites from 2014 to 2020. Systematic differences in reflectivity are found, with ground radar reflectivity on average 2.4 dB smaller than that of the DPR (DPR Version 6). This research found the discrepancies between WSR-88D and DPR arise from different calibration standards, signal attenuation correction, and differences in the ground and space-borne scattering volumes. The recently updated DPR Version 7 product improves rain detection and attenuation corrections, effectively reducing the overall average WSR-88D and DPR reflectivity differences to 1.0 dB. The goal of this study is to examine the systematic differences of radar reflectivity between the NOAA WSR-88D network and the NASA-JAXA spaceborne radar DPR, and to draw attention to radar-application users in recognizing their differences. Further investigation into understanding and alleviating the systematic bias between the two platforms is needed.

CAPSULE (BAMS ONLY)

Consistently smaller radar reflectivities are found in NOAA's ground-based radars, compared to NASA-JAXA's spaceborne radar after adjustment. The difference is reduced when Version 7 DPR product is used.

Accepted for publication in *Bulletin of the American Meteorological Society.* DOI 10.1175/BAMS-D-22-0127.1.

Weather radars have deepened our understanding of precipitation microphysics, improved quantitative precipitation estimates, and severe weather forecasts and warnings (Crum and Alberty, 1993; Hong and Gourley, 2018; Weber et al., 2021; Zhang et al., 2016). In the United States, the well-known Weather Surveillance Radar – 1988 Doppler (WSR-88D) network, operated by the National Oceanic and Atmospheric Administration (NOAA), provides a quasi-continental coverage of high-quality observations of weather events (Crum and Alberty, 1993). Since 2013, all WSR-88D radars have been upgraded to include polarimetric capabilities, leading to an improved understanding of storm microphysics, the development of polarimetric hydrometeor classification algorithms, and enhanced precipitation retrieval techniques (Ryzhkov and Zrnic, 1998; Zhang et al., 2001). However, ground-based radars (denoted as GR herein) suffer from beam blockages, particularly in mountainous regions, that can impede real-time observations of severe weather events (Gabella et al., 2006, Wen et al., 2013). Furthermore, the vertical resolution of operational GRs is degraded by the limited number of elevation angle scans that comprise a radar volume, as well as beam broadening at distant ranges from the radar (Cao et al., 2013, Wen et al., 2013, 2016). In contrast, space-borne radars (SR), such as the CloudSat and the GPM/DPR (Global Precipitation Measures/Dual-frequency Precipitation Radar), provide datasets that are not affected by the same problems that often impact GR data quality. For example, SRs have a less restricted view of the upper rain column and provide enhanced vertical resolutions when compared to GRs. SRs are also well suited to fill the voids where GR coverage is either missing or poor, such as over the ocean or remote areas on land (Battaglia et al., 2019). On the other hand, the temporal sampling rate provided by a single SR for a given location is quite poor when compared to that provided by a GR. Furthermore, the horizontal resolution provided by a SR is limited by the antenna size while the swath width is restricted by considerations of surface clutter and sampling frequency. Given these different advantages and disadvantages, it is clear that the synergetic use of GRs and SR provides a promising opportunity to probe precipitation microphysics (Liao et al., 2005, 2011, Wen et al., 2013).

After the success of the Tropical Rainfall Measurement Mission (TRMM) in 1997, the GPM Core Observatory (CO) - a collaborative effort by The National Aeronautics and Space Administration (NASA) and Japan Aerospace Exploration Agency (JAXA) – was launched in 2014 with the broad goal of enhancing predictive tools for weather and climate (Hou et al., 2014; Li et al., 2020, 2021, 2022; Foufoula-Georgiou et al., 2020; Wen et al., 2016). The

Accepted for publication in *Bulletin of the American Meteorological Society.* DOI 10.1175/BAMS-D-22-0127.1.

GPM CO carried two advanced instruments: the Microwave imager (GMI) and the Dual-frequency Precipitation Radar (DPR), operating at Ku (13 GHz) and Ka (35 GHz) band, and had a one goal of extending the measurement range of light rain and snowfall to an expanded coverage area from 65 S to 65 N (Skofronick-Jackson et al., 2017).

Since its launch in 2014, the GPM DPR has generated great interest in the community by providing not only the quasi-global observations of the precipitation structure, but also the fine vertical resolution to supplement the poor vertical resolution of GRs. This enhanced vertical resolution is especially important in understanding precipitation microphysics, such as precipitation type, hydrometeor identification, and bright band detection (Cannon et al., 2017; Casella et al., 2017; Iguchi et al., 2018; Le et al, 2016; Toyoshima et al., 2015). For example, Cannon et al. (2017) used the capability of the DPR, vertical pointing GRs, and model simulations to identify the melting layer during atmospheric river events in California. Furthermore, precipitation estimates by DPR also serve as a reference database for the Level-3 global seamless gridded precipitation product – IMERG (Integrated Multi-satellitE Retrievals for GPM) (Huffman et al., 2020; Kummerow et al., 2015). Owing to its importance, ground validation (GV) of the GPM DPR have been synchronously initiated around the world (Matsui et al., 2013; Morris and Schwaller, 2010; Oki et al., 2020; Schwaller and Morris, 2011). The GV program involves a set of instruments and software to retrieve collocated and coincident measurements - such as reflectivity, particle size distribution (PSD), and precipitation estimates – by matching ground and airborne instrumentation to SRs (Houze et al., 2017; Tang et al., 2017). The Olympic Mountains Experiment (OLYMPEX), for instance, deployed over 20 different instruments on multiple aircraft to compare the vertical structure of precipitation in complex terrain (Houze et al., 2017). Precipitation rates estimated by DPR were also compared to the Multi-Radar Multi-Sensor (MRMS) rain data (Wang et al., 2021; Zhang et al., 2016) over the continental US from 2014 to 2015, where the difference was found to be within 5% for the annual rainfall amount (Oki et al., 2020). However, comparisons of total rainfall amounts do not reveal the capabilities and deficiencies of the GRs and SRs. Numerous studies have focused on comparing the raw radar reflectivities from GRs and SRs and have explored possible reasons for the observed differences, including calibration procedure and methods of attenuation correction (Anagnostou et al., 2001; Biswas et al., 2018; Cao et al., 2013; Chandrasekar et al., 2003; Keem et al., 2019; Liao et al., 2022; Masaki et al., 2020; Protat et al., 2022). SRs are

Accepted for publication in *Bulletin of the American Meteorological Society.* DOI 10.1175/BAMS-D-22-0127.1.

used as a valid source to calibrate GRs because of the stability of the DPR calibration over time (Protat et al., 2022; Warren et al., 2018; Masaki et al., 2015, 2020).

Despite the significant collective efforts of the many investigations, few studies have attempted to conduct a large-scale comparison of GPM DPR and WSR 88D three-dimensional radar reflectivity in the US. A single or even a limited number of sites do not provide a comprehensive understanding of the differences between the two systems or how they might be jointly used to improve our understanding of microphysical processes. Motivated by the need to use the two radar system synergistically, in this study we attempt to map all available DPR data since its launch and all available WSR-88D GRs from 2014 to 2020 to a common grid with the objectives of: 1) exploring whether systematic differences exist between the DPR and WSR-88D systems, 2) examining whether those differences are consistent for various microphysical processes, 3) determining the primary factors responsible for any systematic differences, and, 4) determining the extent to which the latest DPR (Version-7) product improves the GR-SR comparisons. In this paper, the primary comparisons are made with Version 6 while Version 7 is used to check the degree of improvement in the latest version of the DPR algorithm.

WSR-88D radar

The WSR-88D radar network, operated at the NOAA/National Weather Service (NWS), consists of ~160 operational radars that guidance for nowcasting and warnings (Ansari et al., 2018). The radars, which operate with frequency between 2.7 and 3 GHz (S band), are routinely calibrated and quality controlled by both on-line and off-line calibrations, with the on-line calibration being performed automatically while the system is operating and the off-line calibration routinely performed as needed by maintenance technicians at Preventative Maintenance Intervals (PMI). The data examined as part of the calibration include system noise, system linearity, transmitter power, klystron delay, antenna gain, transmitter frequency, and many other variables (Free et al., 2006).

The WSR-88D system generates three-level products for public access. Level 1 consists of raw signal data at each radar site. Level 2 data are processed Level 1 data, consisting of range gates that have a gate and azimuthal angle resolution of 250 m and 0.5 deg., respectively. Examples of Level 2 base data include radar base reflectivity (Z), velocity, spectrum width, and polarimetric variables differential reflectivity, specific phase, and

Accepted for publication in *Bulletin of the American Meteorological Society.* DOI 10.1175/BAMS-D-22-0127.1.

correlation coefficient. Level 3 products are generated from Level 2 data using advanced algorithms to derive hydrometeor types, precipitation estimates, melting layer location and height. In contrast to Level 2 data, Level 3 data are averaged into different spatial resolution for each variable. In this study, we retrieved the Level 2 base reflectivity and Level 3 hydrometeor types archived at the Amazon S3 bucket (https://registry.opendata.aws/noaa-nexrad/) and Google Cloud Storage (https://cloud.google.com/storage/docs/public-datasets/nexrad).

The Level 3 hydrometeor type product used in this study is generated by a fuzzy-logic based Hydrometeor Classification Algorithm (HCA) (https://www.icams-portal.gov/publications/fmh/FMH11/fmh11partC.pdf) (Park et al., 2009). The HCA has 12 classes, defined according to prescribed thresholds by polarimetric variables. These classes are biological scatters, ground clutter, ice crystals, dry snow, wet snow, light/moderate rain, heavy rain, big drop, graupel, hail mixed with rain, unknown, and no data.

GPM-DPR

This study uses the DPR Precipitation Profile product Version 6 (V6 herein) and Version 7 (V7 herein), released in 2017 and 2022, respectively (Iguchi and Meneghini, 2017, 2021a). In this study, the primary assessment is made using the V6 product from 2015 to 2020, while V7 is used to examine the relative improvements from V6 (Iguchi, 2020). The DPR consists of the Ku-band precipitation radar (KuPR) and Ka-band precipitation radar (KaPR). KuPR and KaPR in V6 have three scanning modes: Normal Scan (NS), High-sensitivity Scan (HS), and Matched Scan (MS). The NS is solely applied to KuPR (similar to TRMM PR), hence it is referred to as KuNS. The HS and MS provide reflectivity estimates based on KaPR, hence they are referred to as KaHS and KaMS, respectively. The KuNS scans the full swath, while the KaPR (KaMS and KaHS) scans only the inner swath prior to May 2018; after May 2018, the KaHS interleaved scan was shifted to the outer swath so that Ka-band data, matched to the Ku-band, became available over the full swath (Liao et al., 2021). The range resolution for KuNS and KaMS is 0.25 km but oversampled at 0.125 km. The KaHS has a range resolution of 0.5 km and a sampling resolution of 0.25 km.

The DPR V7 data, which were released in 2022, had major updates to the data format to reflect the change in the Ka-band scanning. The new data format, called the Full Scan (FS), is used for both frequencies with 176 range-bin arrays and 49 angle-bin arrays. The algorithms

Accepted for publication in *Bulletin of the American Meteorological Society.* DOI 10.1175/BAMS-D-22-0127.1.

include several major improvements, including: (1) better sidelobe rejection; (2) application of the Dual frequency technique to the full swath of 49 angle bins; and, (3) better rain and bright band (BB) detection (Iguchi, 2020, 2021b). To circumvent the ground clutter problem at off-nadir incidence angles (Kubota et al., 2018), we choose only the ten cross-track bins centered at nadir. This is similar to the approach by Cannon et al. (2017).

The three-dimensional attenuation-corrected reflectivity (KuNS) in V6/V7 (zFactorCorrected/zFactorFinal) is used in this study for comparison with S-band GR reflectivity. In contrast to the measured reflectivity (zFactorMeasured), the zFactorCorrected/zFactorFinal accounts for the attenuation suffered from clouds, atmospheric gases, and precipitation (Meneghini et al., 2021). In contrast, the S-band WSR-88D radar with its longer wavelength is relatively immune to attenuation from atmospheric signals (Biswas and Chandrasekar, 2018). Wen et al. (2011) specifically attributed the bias between KuPR and S-band GR to errors in the KuPR attenuation correction. In addition, the BB height, BB top height, BB bottom height, and precipitation type, documented as "BBheight", "Bbtop", "Bbbottom", "typePrecip", respectively, are retrieved to break down the differences in microphysical processes. The presence of BB in the Classification Module is jointly determined by KuPR reflectivity and dual-frequency ratio (DFRm). Readers are referred to Iguchi et al. (2018) and Le et al. (2016) for detailed descriptions. The precipitation type (stratiform, convective, and others) is dependent upon the presence of BB and reflectivity thresholds.

Volume matching

Because of different viewing geometries of the DPR and WSR-88D, a direct comparison of their data is not feasible without resampling one or both datasets. Common approaches to reconcile the two systems differences are: (1) mapping GR variables onto 3D cartesian coordinates (Anagnostou et al., 2001; Liao and Meneghini, 2009; Schwaller and Morris, 2011) and (2) retrieving intersected radar rays called volume-matching (Biswas and Chandrasekar, 2018; Wen et al., 2011). In this study, we applied the volume-matching method, as illustrated in Fig. 1. One sample bin, highlighted in the red hatched area, is overlaid by both DPR and GR radar beams. To determine the bin height (relative to the surface), the vertical datum of both systems needs to be standardized. We convert the DPR vertical datum – geoid – to the WSR-88D datum (NAVD88 – North America Vertical Datum 1988). Practically, the GR gate height is calculated by the radar site elevation plus the relative

Accepted for publication in *Bulletin of the American Meteorological Society.* DOI 10.1175/BAMS-D-22-0127.1.

height determined by the elevation angle and distance to the site. For the DPR, we first calculate the elevation of each bin using the available flight information (ellipsoidal elevation offset, local zenith angle, and bin number) (Iguchi et al., 2018). Next, we convert the height at the elliptical geoid to the height at the NAVD88. For variables inside the common bin, we average numerical values such as the reflectivity (in linear units), and BB height. For categorical data such as hydrometer type, we search for the most dominant type (maximum occurrence) within the volume and assign it in our database. Detailed descriptions of the volume matching method can be found in Morris and Schwaller (2010).

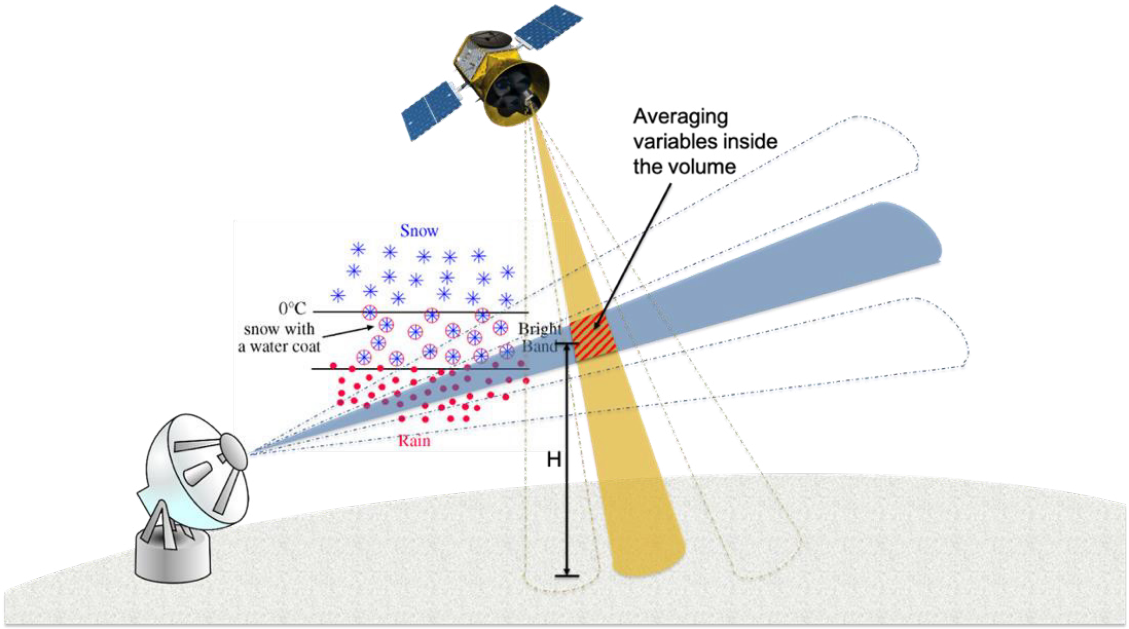

Fig. 1. Schematic illustration of 3D volume matching for GPM DPR and Ground Radar.

Event selection

To accelerate data processing and minimize storage issues, we consider only significant precipitation events that appear in the NWS storm database (https://www.ncdc.noaa.gov/stormevents/) (Li et al., 2022). Only recorded precipitation events that occurred within a range of 25-100 km of the individual radar site are considered; this mitigates the GR blind spot near the radar, the non-uniform beam filling issue due to beam broadening, and radar wave bending in the stratified atmosphere. In addition, as noted above, an event must be located within the 10 DPR angle bins centered around nadir within 10 minutes of the satellite overpass. With these restrictions, there are in total over two million samples suitable for this study. The number of samples per radar site is shown in Fig. 2. This result, in principle, reflects the precipitation climatology of the continental US (CONUS),

Accepted for publication in *Bulletin of the American Meteorological Society.* DOI 10.1175/BAMS-D-22-0127.1.

where most of the precipitation falls in the Pacific Northwest and east of the Mississippi. In contrast, arid regions like the Southwest have a limited number of samples. A minimum sample size of 1,000 is required for further analysis.

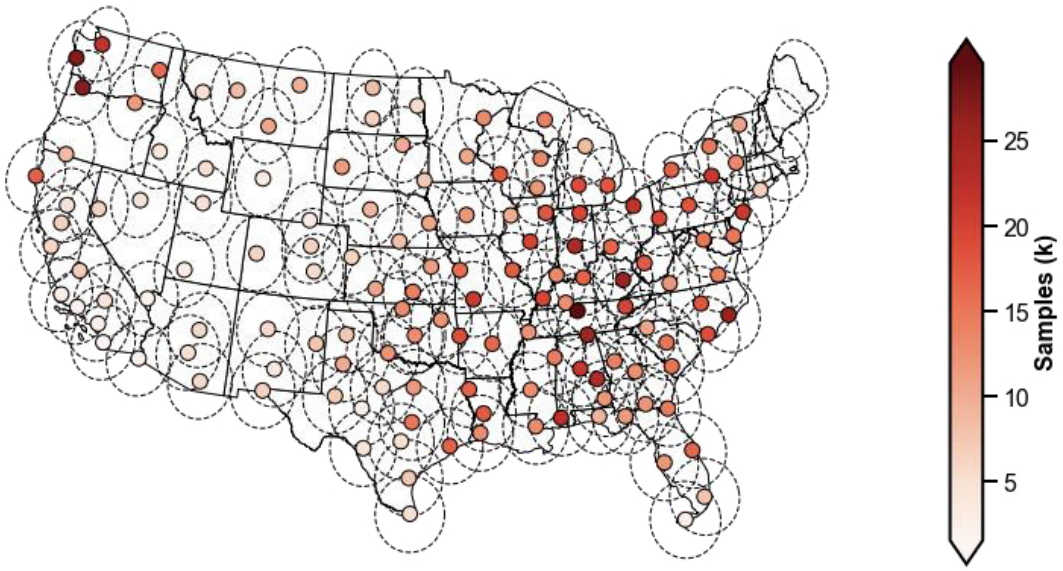

Fig. 2. Number of samples (in thousand) collected at each radar site. Dashed circles represent the detectable radar range (~300 km).

Ku-S band reflectivity adjustment

Several approaches have been discussed in the literature to account for the different backscattering characteristics of hydrometeors for S-band (Rayleigh scattering) and Ku-band radar (non-Rayleigh scattering) (Cao et al., 2013; Chandrasekar et al., 2003; Liao et al., 2005; Liao and Meneghini, 2009a; Wen et al., 2011). These approaches include but are not limited to (1) empirical relations that convert the S-band reflectivity to that at Ku-band for rain, snow, the melting layer (Cao et al., 2013; Liao et al., 2009b), and (2) microphysical and scattering models for different hydrometeors (Wen et al., 2011; Biswas and Chandrasekar, 2018). The dual-frequency ratio (DFR), defined as the ratio between S-band GR and Ku-band DPR, is a function of hydrometeor shape, size, and phase (Cao et al., 2013; Iguchi et al., 2018; Liao et al., 2005, 2011). The DFR, as given in Eq. 1, is equal to the difference in reflectivity factors, in dB, between the two frequencies.

$$DFR = 10log_{10}Z_{GR} - 10log_{10}Z_{DPR} \quad (1)$$

Liao et al. (2009b) showed that the Ku-band reflectivity factor tends to be larger than the S-band reflectivity factor in rain but smaller in snow. Cao et al. (2013) later extended this

Accepted for publication in *Bulletin of the American Meteorological Society.* DOI 10.1175/BAMS-D-22-0127.1.

relation to the melting layer, which is often characterized by the BB in radar data, by fitting a polynomial function. In this study, we utilize the relations established by Cao et al. (2013) to account for the reflectivity differences for rain, snow, hail, and the melting layer. A generic equation is shown in Eq. 2, where the DFR is expressed as a fourth-order polynomial function of the S-band GR reflectivity. The empirical parameters $a_0 - a_4$ can be found in Cao et al. (2013). The $a_0 - a_4$ parameters are variable with different hydrometeors, i.e., rain, dry snow, dry hail, melting snow, and melting hail.

$$DFR = a_0 {Z_{DPR}}^0 + a_1 {Z_{DPR}}^1 + a_2 {Z_{DPR}}^2 + a_3 {Z_{DPR}}^3 + a_4 {Z_{DPR}}^4 \quad (2)$$

Note that all the comparisons in our results were done after adjusting the reflectivity differences.

We use three metrics throughout this study to represent the differences of reflectivity between DPR and GR: bias, Root Mean Square Difference (RMSD), and Spearman Correlation Coefficient (CC) as their formulas shown in Eq.3-5.

$$bias = \frac{\sum_{i=1}^{n}(Z_{DPR} - Z_{GR})}{n} \quad (3)$$

$$RMSD = \sqrt{\frac{1}{n}\sum_{i=1}^{n}(Z_{DPR} - Z_{GR})^2} \quad (4)$$

$$CC = \frac{Cov(\mathrm{R}(Z_{GR}),\mathrm{R}\,(Z_{DPR}))}{\sigma_{(Z_{GR})}\sigma_{(Z_{DPR})}}, \quad (5)$$

where n is the total number of sample sizes, *R*(GR) is the rank of GR, and *R*(DPR) is the rank of DPR.

Results

Systematic view of reflectivity

The volume matched reflectivities are sampled at each WSR-88D radar site, and the mean differences are illustrated in Fig. 3. Each radar site indicates a positive bias (Z_DPR> Z_GR) across the CONUS, indicating a consistent and systematic positive difference between the DPR and WSR-88D systems. The average reflectivity difference from the 136 radar sites is 2.4 dB, consistent with the results reported by Biswas and Chandrasekar (2018) in which the differences were found to be between 2 and 3 dB at five GR sites. They attributed the difference to the non-Rayleigh scattering evident in Ku-band DPR wavelength. Keem et al. (2019) reported a 2.27 dB difference at three radar locations in Iowa. They explained that the

Accepted for publication in *Bulletin of the American Meteorological Society.* DOI 10.1175/BAMS-D-22-0127.1.

difference was related to GR wet radome attenuation and beam blockage. In other regions, Warren et al. (2018) found an average 4.0 dB difference between three Australian GRs and DPR, in contrast to 0.1 dB difference for TRMM PR. D'Adderio et al. (2021) recently reported a positive bias ranging from 2.19 dB to 5.57 dB for the three C-band radars in Italy. Despite the variability in the results, almost all studies indicate a significant positive difference between the DPR V6 and GR.

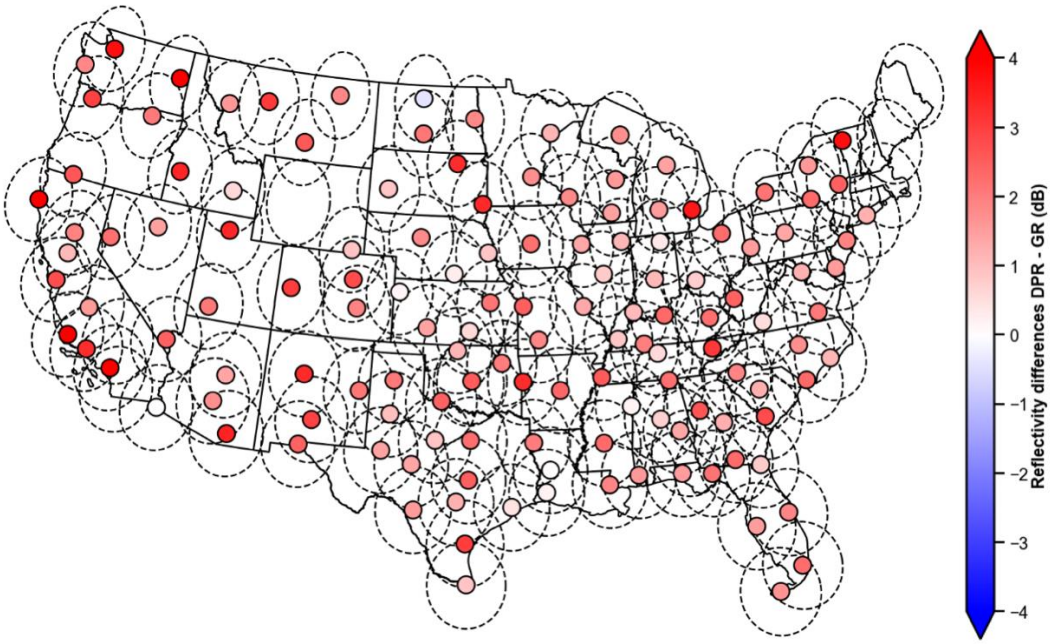

Fig. 3. Spatial map of reflectivity differences (DPR minus GR) in dB at WSR-88D site.

Figure 4 depicts the grouped reflectivity differences for 136 WSR-88D sites. Overall, the majority of the GRs (77.2%), as depicted by the cyan color in Fig. 4, have absolute differences of less than 3 dB, indicating "good" agreement. Those GRs are mainly located in the central US, Southeast, and East Coast. Around 19.8% of the GRs fall into the second category (difference of 3-5 dB), scattered over the CONUS. Only four radars have severe differences (>5 dB), all located in the southern California. The limited sample size for these radars (as shown in Fig. 2) is a possible reason for the large deviations. In general, radars in mountainous regions such as the Rockies disagree with DPR more, partly due to beam blockage that can result in a severe reduction of GR reflectivity values.

Accepted for publication in *Bulletin of the American Meteorological Society.* DOI 10.1175/BAMS-D-22-0127.1.

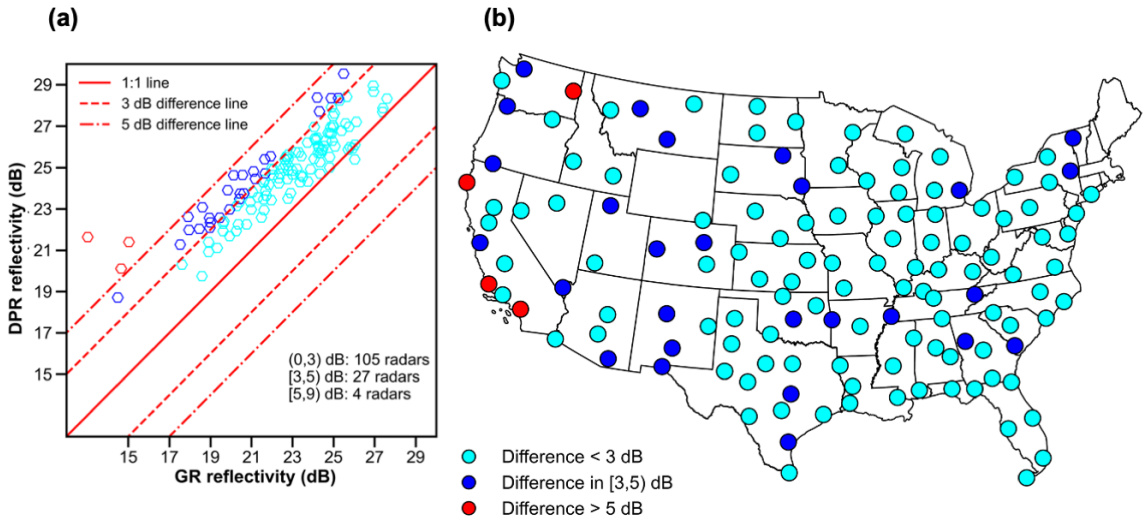

Fig. 4. Reflectivity differences categorized at three bins: 0-3, 3-5, and 5-9 dB. Figure shows (a) scatter plot of DPR reflectivity and GR reflectivity at 140 WSR-88D radar locations, and (b) map of WSR-88D locations with color-coded category. Dots are color-coded by category.

Aggregated by hydrometeor types

The effective radar reflectivity is determined by the combination of the PSD and the backscattering cross section of the hydrometeors (Chandrasekar et al., 2003; Liao et al., 2009; Wen et al., 2011). We group reflectivity values with respect to eight major hydrometeor types, as shown in Fig. 5. Although the correlation is as high as 0.86 for all types combined, a bias is also obvious (+1.98 dB) with the bulk of the samples above and parallel to the 1:1 line. Of these types, light/moderate precipitation and big drops have high positive biases of 1.94 and 1.86 dB, respectively. Solid precipitation, i.e., dry/wet snow and graupel, have a higher positive bias, when compared to liquid precipitation, ranging from 1.97 to 3.64 dB. This cannot be explained by the difference in the backscattering cross sections at different wavelength nor by signal attenuation (Wen et al., 2011). We suspect the positive bias is related to the different calibration procedures used for the two radar systems. One typical example is in ice crystal or dry snow regions where the DPR signal at the storm top is relatively attenuation-free, implying that calibration is the main sources of the difference (Liao and Meneghini, 2009). On the other hand, heavy rain and hail with rain exhibit negative biases (-0.31 and -0.33 dB, respectively), which might be caused by under-correction of attenuation in heavy rain and hail counteracting the calibration differences.

Accepted for publication in *Bulletin of the American Meteorological Society*. DOI 10.1175/BAMS-D-22-0127.1.

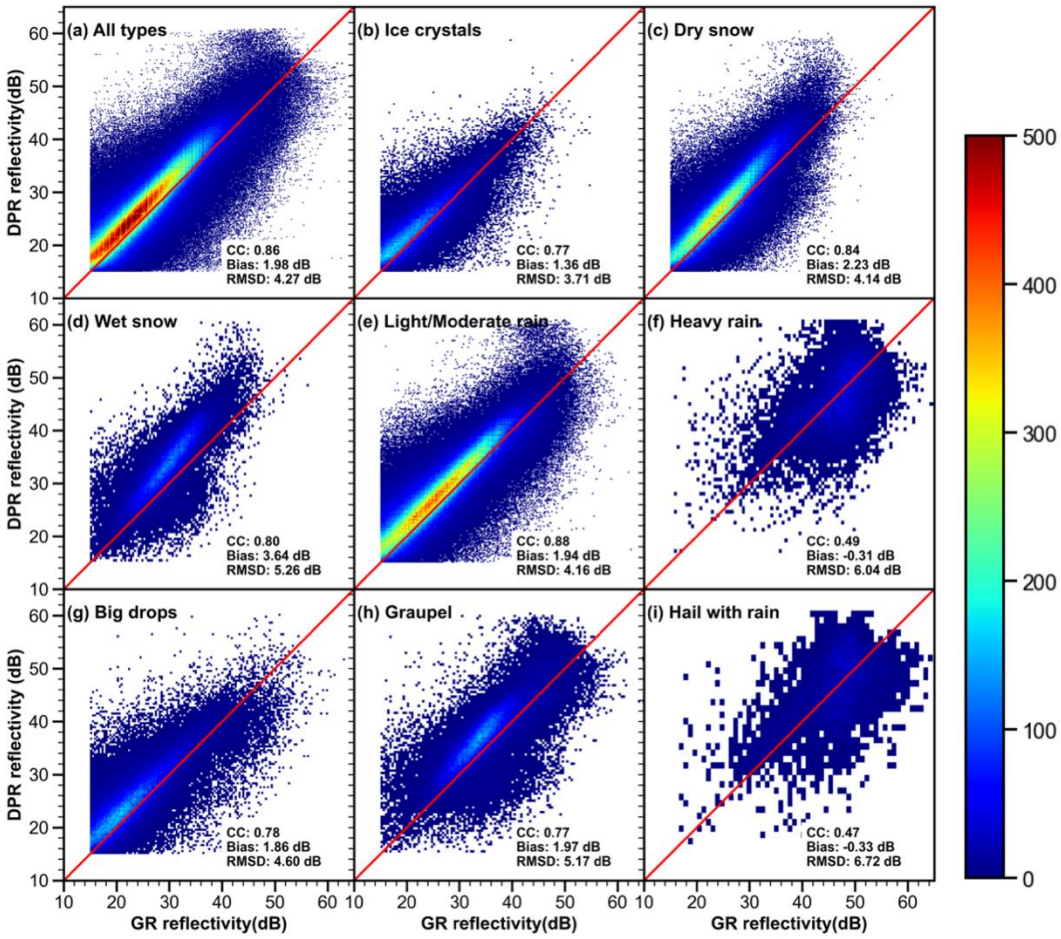

Fig. 5. Reflectivity comparisons by different hydrometeor types at all WSR-88D sites.

Comparisons by precipitation types

Figure 6 depicts the comparisons categorized by different precipitation types as determined by the DPR. Overall, the results grouped by both GR (Fig. 5) and DPR (Fig. 6) depict positive biases of the DPR relative to the GR. It also shows that the reflectivity for the two radars, which is centered around the 1:1 line, aligns reasonably well in convective precipitation. The positive bias is thus reduced to be within 1.5 dB. Nevertheless, the reflectivity in stratiform precipitation starts to deviate, with a positive bias of 1.3 dB. More importantly, the difference becomes greater when the reflectivity values estimated by the GR are taken to be larger than 30 dB, as highlighted in the red box (Fig. 6). To further analyze this example, we separate the stratiform precipitation relative to its location with respect to the BB height as shown in Fig. 7.

Accepted for publication in *Bulletin of the American Meteorological Society.* DOI 10.1175/BAMS-D-22-0127.1.

Above the BB, there is a positive bias (1.19 dB) that can be attributed to calibration differences. Within the BB, the bias (1.14 dB) is the smallest among all of the cases, yet the RMSD is the largest. The intrinsic positive bias is possibly compensated by under-corrected attenuation within the BB. Below the BB, the bias increases to 1.6 dB, and samples deviating from the 1:1 line show again the elevated tail highlighted in the red box (Fig. 7), which correlates with the large bias in light/moderate rain in Fig. 5e. Despite a positive bias, the CC (0.89) and RMSD (3.37 dB) below the BB are the best among the metrics in the three regions.

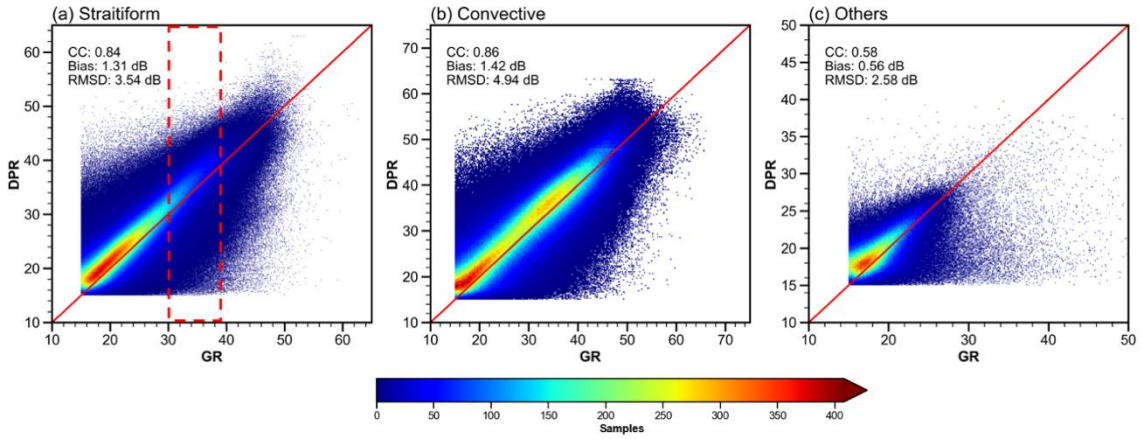

Fig. 6. Reflectivity comparisons by precipitation types for: (a) stratiform precipitation; (b) convective precipitation; (c) others. The red rectangle highlights the region where the high-density samples start to deviate from the 1:1 line.

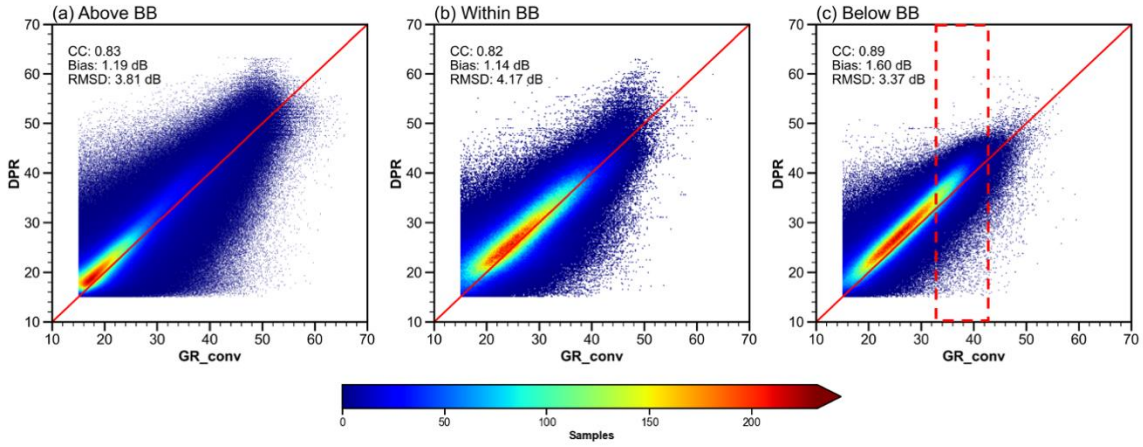

Fig. 7. Similar to Fig. 6, but for reflectivity comparisons by height relative to the bright band (BB). (a) beam height above the BB; (b) beam height within the BB; (c) beam height below the BB.

Accepted for publication in *Bulletin of the American Meteorological Society.* DOI 10.1175/BAMS-D-22-0127.1.

One way to check the accuracy of the DPR attenuation correction is to compare vertical profiles of reflectivity between DPR and GR. If the magnitude of differences between DPR and GR increases/decreases monotonically with the DPR range, it would suggest the DPR under/over-corrects attenuation. We regrouped the reflectivity values at bins with height above the ground from 1500 to 5700 m in intervals of 200 m. The median value and uncertainty range (from 25th percentile to 75th percentile) are shown from each bin as shown in Fig. 8. Note that since the results integrate and smooth all events that have varying BB heights, a typical stratiform profile is not obvious in this case.

We find a constant shift (~3 dB) between DPR and GR reflectivity from top to bottom for stratiform precipitation, indicating that attenuation correction of the DPR is reasonable. The reflectivity variability range for DPR begins to narrow at the top (5 dB) yet increases to around 10 dB at the bottom. The range of reflectivity in GR is narrower than that of DPR, despite an increase in the middle which is possibly related to melting processes. For convective precipitation, however, the bias is around 3 dB at the top and 1 dB at the bottom height. This suggests a slight under-correction (~2 dB) of the DPR attenuation for convective precipitation. The reflectivity range, though much greater than stratiform precipitation as expected, follows the same pattern – increasing from the top to the bottom. Again, DPR has a larger reflectivity range than GR, which is probably related to the coarse vertical resolution of GR and signal noise of DPR such as sidelobe, ground clutter, or atmospheric attenuation as signals penetrate deep into the storm.

Accepted for publication in *Bulletin of the American Meteorological Society.* DOI 10.1175/BAMS-D-22-0127.1.

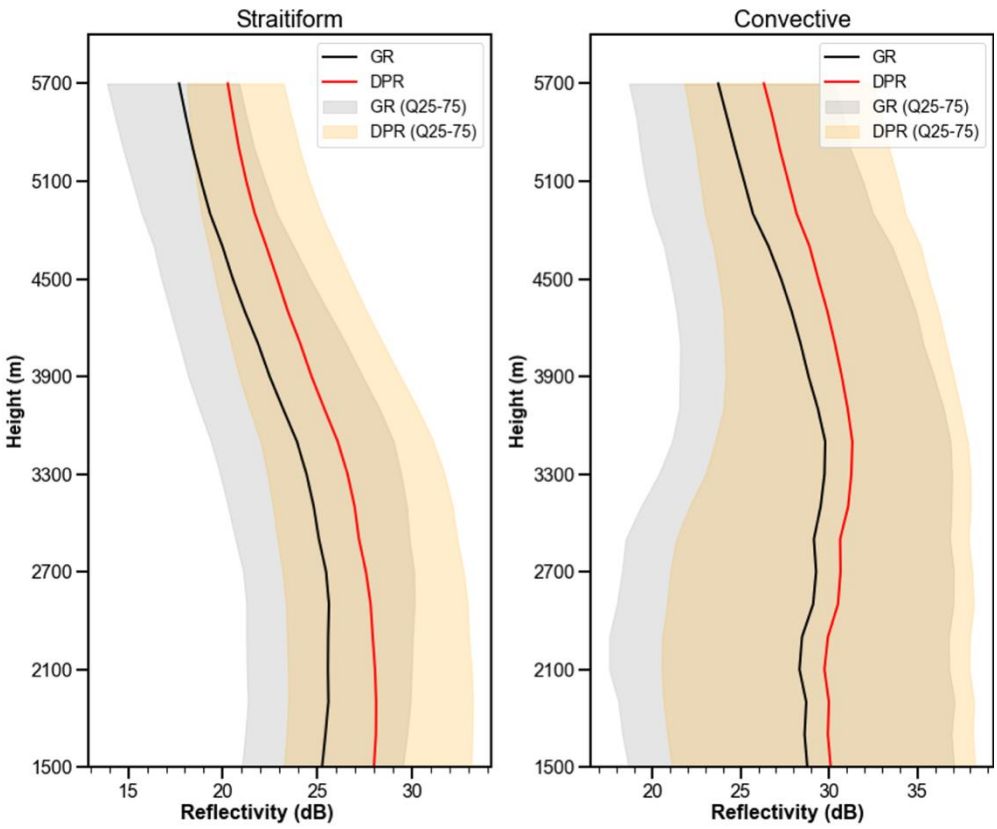

Fig. 8. Vertical profile of reflectivity for DPR and GR in stratiform rain and convective rain. The shaded color represents uncertainty range, quantified between 25th percentile and 75th percentile.

Comparisons to the NASA Validation Network data

To confirm our matching methods, we compared our matched results with the NASA Validation Network (VN) data that is publicly accessible (Gatlin et al., 2020; Keem et al., 2019; Schwaller and Morris, 2011). We processed volume-matched VN dataset from DPR and GR from 2014 – 2021 at all matched WSR-88D sites (only in the eastern US). To make a fair comparison, we applied the same reflectivity conversion from Ku band to S band, as mentioned in Section 2.5. In contrast to our matching method, VN has stringent data selection protocols. For instance, radar data with non-uniform beam filling greater than 10% are ignored (Schwaller and Morris, 2011). In our case, we select events based on the storm reports as mentioned in Section 2.4. In the VN algorithm the radar variables are sampled onto a 3D cartesian coordinates, while we use a direct volume matching method.

Comparisons of reflectivity from all available sites show positive bias (DPR > GR), with the bias being 1.91 dB for VN data and 2.01 dB for our data. From Fig. 4b, we see that most

Accepted for publication in *Bulletin of the American Meteorological Society.* DOI 10.1175/BAMS-D-22-0127.1.

of these radar sites have relatively "good" agreement with DPR, with the biases below 3 dB. However, other radar sites in the western US are not included in the current VN data.

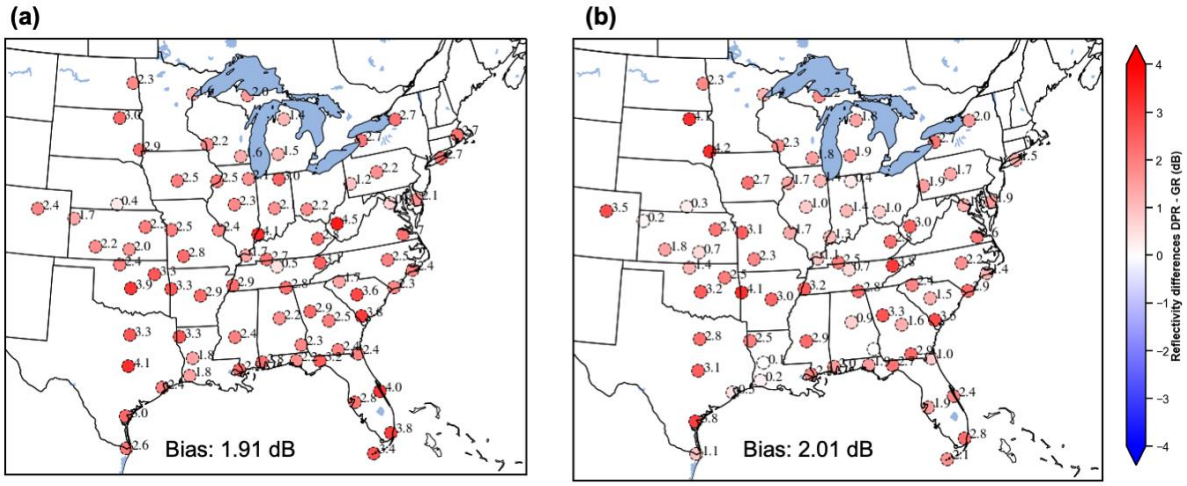

Fig. 9. Map of reflectivity bias for (a) NASA Network Validation data (b) our method.

Possible reasons for the DPR and GR differences

In this section, we discuss the most probable driving factors that are responsible for the DPR-GR differences. First, the primary factor is believed to be calibration differences as, for example, seen in Fig. 5, where a positive bias is prominent in the ice regions that are attenuation-free. The DPR and WSR-88D radars adopt different calibration protocols. The DPR has implemented the so called "internal" and "external" calibration to ensure the received signal is correctly converted to reflectivity factor (Masaki et al., 2020; Oki et al., 2020). The internal calibration ensures that power losses from the transmitter to receiver are accounted for, and the external calibration, considering the DPR as a whole system, calibrates signals from ground to the DPR, also called absolute calibration. The internal calibration determines the slope of the transfer function while the external calibration determines the intercept (Masaki et al., 2020). The WSR-88D radars routinely conduct coherent calibration procedures at each radar site, adjusting time-varying system noise, reflectivity correction factors (on-line calibration), and slowly varying parameters (offline calibration) (Free et al., 2006). Meanwhile, external calibration is conducted using either a self-consistency test (Ryzhkov et al., 2005) or by comparisons to ground-based instruments (e.g., disdrometers) on a regular basis. We found a 1.9 dB shift in the regions above the BB. We suspect that there is a disagreement of the intercept in the transfer function, which is determined by external calibration for both systems.

Accepted for publication in *Bulletin of the American Meteorological Society.* DOI 10.1175/BAMS-D-22-0127.1.

Second, the attenuation correction to the DPR Ku-band measured reflectivity plays a central role in the reflectivity differences. The latest Surface Reference Technique (SRT) is applied as a primary method in path-integrated attenuation (Meneghini et al., 2021). Although the SRT itself is independent of precipitation phase, the allocation of gate corrected reflectivity entails phase information, which is classified based on DFR. Yet, without attenuation-corrected reflectivity, it is difficult to compute DFR and classify precipitation phase correctly (Iguchi et al., 2018). Although this concern is less severe in stratiform rain where precipitation phase can be inferred given the location of bright band, the issue is more problematic in convective rain as is the NUBF effect that influences all the attenuation estimates. Another method of attenuation correction – the Hitschfield-Bordan method – works well for light rains and small-to-moderate attenuation, yet it still suffers from the phase-state problem in convective rain. In summary, the status quo is that the current algorithm does not handle the attenuation correction issue to the degree that would be desired, and there are ongoing efforts to improve this.

Third, differences in radar scanning and radar characteristics hinder the match between the two. Problems such as NUBF depend on the dimension of the volume chosen to resample radar rays. Particularly for GRs, poor vertical resolution and beam broadening as the distance from the radar increases worsen the NUBF effect, which is further exacerbated in complex terrains (Ryzhkov, 2007). Recent studies have been seeking data-driven approaches to mitigate the beam blockage effect in occlusive areas, which have potential to overcome this problem (Yin et al., 2021).

In this study, we provide the first evaluation of the latest version of the DPR algorithm. Similar plots to Figs. 3-8 are shown in the Supplementary plots Figs. S1-6. We also summarized the improvements of bias in Table 1. A continental map shown in Fig. S1 manifests a good overall improvement showing that the systematic bias between the DPR and GR is reduced in V7. In particular, the average reflectivity difference is reduced from 2.4 dB (V6) to 1.0 dB (V7), where in all cases the DPR exceeds the GR. The number of radar sites that have reflectivity differences within 3 dB has increased from 105 (V6) to 131 (V7), an increase of 24.8% (Fig. S2). The overall bias by hydrometeors has decreased from 1.98 dB (V6) to 1.37 dB (V7), and can be attributed to an improvement in dry snow DPR estimates (RMSD – 4.1 vs. 3.9 dB; bias – 2.23 vs. 1.01 dB) and wet snow (RMSD – 5.3 vs. 3.7 dB; bias – 3.64 vs. 1.45 dB) (Fig. S3). However, persistent differences in light/moderate rains are

Accepted for publication in *Bulletin of the American Meteorological Society.* DOI 10.1175/BAMS-D-22-0127.1.

present in V7, with 2.01 dB bias comparable to V6 (1.94 dB). Biases with regard to rain type have been decreased in V7 (Fig. S4), and also for heights above BB (Fig. S5). For heights within BB and below BB, there are small increases in biases. The vertical profile shown in Fig. S6 now has a narrower gap (3 dB for V6 vs. 0.8 dB for V7) and larger overlapping areas. Overall, the improvements from V6 to V7 are substantial and constitute a closer match between GPM DPR and WSR-88D GR. The improvements are primarily ascribed to (1) advances in path-integrated attenuation (PIA) correction, (2) adoption of an improved sidelobe clutter correction scheme (Kanermaru et al., 2021; Seto et al., 2022), and (3) changes in the DPR solver module including use of a range-adjustable parameter (epsilon).

The presence of soil moisture can modify the surface backscattering cross section and introduce errors in the estimate of path attenuation. While there is no adjustment in V6, in V7 (Iguchi et al., 2021b; Seto et al., 2022), an account of this effect tends to increase the rain rate estimates over land. Second, the sidelobe clutter correction is improved, especially when a BB is present near the surface. This improved filtering decreases the bias. Third, the updated epsilon parameter affects the Drop Size Distribution, and thus the attenuation. Despite overall improvement, there is still a significant difference, when considering that a difference of 1 dB in radar reflectivity can produce a change of 15% in rain rates (Nakamura, 2021).

Table 1. Summary of bias between GPM DPR Version 6 and Version 7 (numbers with bolded format indicate better performance).

Difference according to aggregation levels		V6	V7
Continental average DPR-GR difference (dB)		2.4	**1.0**
# Radar sites within 3 dB differences		105	131
Hydrometeor types	Overall	1.98	**1.37**
	Ice crystals	1.36	**1.15**
	Dry snow	2.23	**1.01**
	Wet snow	3.64	**1.45**
	Light/Moderate rain	**1.94**	2.01

Accepted for publication in *Bulletin of the American Meteorological Society.* DOI 10.1175/BAMS-D-22-0127.1.

	Heavy rain	-0.31	**0.14**
	Big drops	1.86	**1.69**
	Graupel	1.97	**0.69**
	Hail with rain	**-0.33**	-0.53
Precipitation type	Stratiform	1.31	**1.24**
	Convective	1.42	**1.12**
	Others	0.56	**0.07**
Relative to Bright Band (BB)	Above	1.19	**0.85**
	Within BB	**1.14**	1.42
	Below	**1.60**	1.78

Concluding remarks and recommendations

Ground-based radars in synergy with spaceborne radars can improve our understanding of cloud and precipitation microphysics. Caution should be taken when using the both GPM-DPR and WSR-88D radars, however, because systematic differences do exist. In this study, we quantify the reflectivity differences from a systematic overview of 136 WSR-88D radars. We find that, on average, the reflectivities from the DPR are greater than those of the WSR-88D radars by 2.4 dB. At a majority (>77%) of the sites, the difference is within a 3 dB. Poorly matched DPR-GRs generally reside either over complex terrain or at the southern California sites, where the sample size is small. An analysis of the results suggests that the discrepancies originate primarily from three sources: (1) different calibration protocols, (2) errors in the DPR attenuation correction, and (3) imperfect matching methods due to differences in the spaceborne and ground-based radar geometries and beamwidths. NUBF effects further exacerbate the attenuation correction and volume matching problems. In the newer version V7, the DPR-GR reflectivity bias is reduced from 2.4 dB (V6) to 1.0 dB (V7). This improvement is the result of a better sidelobe rejection method and better attenuation correction procedures implemented in V7. Closer matches between GR and DPR in wet and dry snow are found in V7, yet differences in light/moderate rains persist.

Accepted for publication in *Bulletin of the American Meteorological Society.* DOI 10.1175/BAMS-D-22-0127.1.

This study aims to highlight the systematic difference between DPR and GR as the interest grows in using a multi-sensor approach to probe clouds and precipitation microphysics. It does not intend to judge which of the two systems is more accurate because each inherits its own strengths and deficiencies. Any future investigation of this topic would benefit from incorporating more radars from around the world. Moreover, the consistency of the Ku-band SR and S-band GR data over time could be addressed by considering TRMM, GPM and WSR-88D data sets over the last two decades. Opportunistic sensors such as CloudSat, RainCube, EarthCARE (to be launched in 2022) will provide more confidence in this task. The Triple Collation method can be used to examine the similarity and difference among the three independent products without assuming ground truth (Li et al., 2020).

Acknowledgments.

We would like to acknowledge NASA Oklahoma EPSCoR Research Initiation Grant. The first author is sponsored by the University of Oklahoma Hydrology and Water Security (HWS) program and Graduate College Hoving Fellowship. We thank NASA Goddard Precipitation Measurement Mission scientist Dr. Toshio Iguchi for his constructive comments. We are also thankful for the support from NASA Marshal Space Flight Center Dr. Patrick Gatlin and Berendes who maintain and provide us VN datasets. Additionally, we thank NOAA/NWS/Radar Operations Center Dr. Dan Berkowitz for his help on WSR-88D radar calibration. We thank three anonymous reviewers for their valuable inputs to improve the quality of this manuscript.

Data Availability Statement.

GPM DPR level 2 Version 06 and Version 07 data can be downloaded from the NASA GES DISC: https://doi.org/10.5067/GPM/DPR/GPM/2A/06 and https://doi.org/10.5067/GPM/DPR/GPM/2A/07. The NEXRAD Level 2 base reflectivity and Level 3 hydrometeor types archived at the Amazon S3 bucket (https://registry.opendata.aws/noaa-nexrad/) and Google Cloud Storage (https://cloud.google.com/storage/docs/public-datasets/nexrad), respectively. Scripts used in this study can be found from the Github repository: https://github.com/chrimerss/GPM_DPR.

Accepted for publication in *Bulletin of the American Meteorological Society.* DOI 10.1175/BAMS-D-22-0127.1.

REFERENCES

Anagnostou, E. N., C. A. Morales, and T. Dinku, 2001: The Use of TRMM Precipitation Radar Observations in Determining Ground Radar Calibration Biases, *J. Atmos. Oceanic Technol.*, **18**, 616-628.

Ansari, S., S. and Coauthors, 2018: Unlocking the Potential of NEXRAD Data through NOAA's Big Data Partnership, *Bull. Amer. Meteor. Soc.*, **99**, 189-204.

Battaglia, A. and Coauthors, 2020: Spaceborne cloud and precipitation radars: Status, challenges, and ways forward. *Rev. Geophys.*, **58**, e2019RG000686, https://doi.org/10.1029/2019RG000686

Biswas, Sounak K., and V. Chandrasekar, 2018: Cross-Validation of Observations between the GPM Dual-Frequency Precipitation Radar and Ground Based Dual-Polarization Radars, *Remote Sens.*, **10**, 1773, https://doi.org/10.3390/rs10111773

Cannon, F., F.M. Ralph, A.M. Wilson, and D.P. Lettenmaier, 2017: GPM satellite radar measurements of precipitation and freezing level in atmospheric rivers: Comparison with ground-based radars and reanalyses. *J. Geophys. Res. Atmos.*, **122**, 747– 12,764, https://doi.org/10.1002/2017JD027355

Cao, Q., Y. Hong, Y. Qi, Y. Wen, J. Zhang, J.J. Gourley, and L. Liao, 2013: Empirical conversion of the vertical profile of reflectivity from Ku-band to S-band frequency, *J. Geophys. Res. Atmos.*, **118**, 1814– 1825, https://doi.org/10.1002/jgrd.50138.

Casella, D., G. Panegrossi, P. Sano, A.C. Marra, S. Dietrich, B.T. Johnson, and M.S. Kulie, 2017: Evaluation of the GPM-DPR snowfall detection capability: Comparison with Cloudsat-CPR, *Atmos. Res.*, **197**, 64-75.

Chandrasekar, V., H. Fukatsu, and K. Mubarak, 2003: Global mapping of attenuation at Ku- and Ka-band. *IEEE Trans. Geosci. Remote Sens.*, **41**, 2166-2176.

Crum, T. D., and R.L. Alberty, 1993: The WSR-88D and the WSR-88D Operational Support Facility, *Bull. Amer. Meteor. Soc.*, **74**(9), 1669-1688.

D'Adderio, L. P., G. Vulpiani, F. Porcù, A. Tokay, A., and R. Meneghini, 2018: Comparison of GPM Core Observatory and Ground-Based Radar Retrieval of Mass-Weighted Mean Raindrop Diameter at Midlatitude, *J. Hydrometeor.*, **19**(10), 1583-1598.

Accepted for publication in *Bulletin of the American Meteorological Society.* DOI 10.1175/BAMS-D-22-0127.1.

Foufoula-Georgiou, E. and Coauthors, 2020: Advancing Precipitation Estimation, Prediction, and Impact Studies, *Bull. Amer. Meteor. Soc.*, **101**(9), E1584-E1592.

Free, A. D., N. K. Patel, and R. W. Macemon, 2006: Open Radar Data Acquisition (ORDA) Calibration Consistency. *22nd Conf. on Interactive Information Processing Systems for Meteorology*, Atlanta, Georgia.

Gatlin, P.N., W.A. Petersen, J.L. Pippitt, T.A. Berendes, D.B. Wolff, A. Tokay, 2020: The GPM Validation Network and Evaluation of Satellite-Based Retrievals of the Rain Drop Size Distribution. *Atmos.*, **11**, 1010, https://doi.org/10.3390/atmos11091010

Gabella, M., J. Joss, G. Perona and S. Michaelides, 2006: Range adjustment for ground-based radar, derived with the spaceborne TRMM precipitation radar, *IEEE Trans. Geosci. Remote Sens.*, **44**, 126-133, https://doi.org/10.1109/TGRS.2005.858436.

Hong, Y., and J.J. Gourley, 2015: *Radar Hydrology: Principles, Models, and Applications* (1st ed.). CRC Press, 176 pp., https://doi.org/10.1201/b17921

Hou, A. Y., R.K. Kalar, S. Neeck, A.A. Azarbarzin, C.D. Kummerow, M. Kojima, R. Oki, K. Nakamura and T. Iguchi, 2014: The Global Precipitation Measurement Mission. *Bull. Amer. Meteor. Soc.*, **95**, 701–722, https://doi.org/10.1175/BAMS-D-13-00164.1.

Houze, R. A. and Coauthors, 2017: The Olympic Mountains Experiment (OLYMPEX), *Bull. Amer. Meteor. Soc.*, **98**(10), 2167-2188.

Huffman, G.J. and Coauthors, 2020: Integrated Multi-satellite Retrievals for the Global Precipitation Measurement (GPM) Mission (IMERG). *Satellite Precipitation Measurement. Advances in Global Change Research*, V. Levizzani, C. Kidd, D.B. Kirschbaum, C.D. Kummerow, K. Nakamura, F.J. Turk, Ed., *Springer*, 343-353.

Iguchi, T. and R. Meneghini, 2017: GPM DPR Precipitation Profile L2A 1.5 hours 5 km V06, Greenbelt, MD, Goddard Earth Sciences Data and Information Services Center (GES DISC), Accessed: 2020/12/15, https://doi.org/10.5067/GPM/DPR/GPM/2A/06

Iguchi, T., N. Kawamoto, and R. Oki, 2018: Detection of Intense Ice Precipitation with GPM/DPR, *J. Atmos. Oceanic Technol.*, **35**(3), 491-502.

Iguchi, T., 2020: Dual-Frequency Precipitation Radar (DPR) on the Global Precipitation Measurement (GPM) Mission's Core Observatory. *Satellite Precipitation Measurement.*

Accepted for publication in *Bulletin of the American Meteorological Society.* DOI 10.1175/BAMS-D-22-0127.1.

Advances in Global Change Research, V. Levizzani, C. Kidd, D.B. Kirschbaum, C.D. Kummerow, K. Nakamura, F.J. Turk, Ed., *Springer*, 183-192.

Iguchi T., and R. Meneghini, 2021a: GPM DPR Precipitation Profile L2A 1.5 hours 5 km V07, Greenbelt, MD, Goddard Earth Sciences Data and Information Services Center (GES DISC), Accessed: 2021/08/01, https://doi.org/10.5067/GPM/DPR/GPM/2A/07

Iguchi, T., Seto, S., Meneghini, R., Yoshida, N., Awaka, J., Le, M., Chandrasekar, V., Brodzik, S., Kubota, T., 2021b: GPM/DPR Level-2 Algorithm Theoretical Basis Document, NASA Goddard Space Flight Center, https://arthurhou.pps.eosdis.nasa.gov/Documents/ATBD_DPR_V07A.pdf

Kanemaru, K., H. Hanado, K. Nakagawa, 2021: Improvement of the clutter removal method for the spaceborne precipitation radars, *IEEE Geosci. and Remote Sens. Soc.*, the International Geoscience and Remote Sensing Symposium 2021, Virtual Symposium

Keem, M., B.C. Seo, W.F. Krajewski and K.R. Morris, 2019: Inter-comparison of reflectivity measurements between GPM DPR and NEXRAD radars. *Atmos. Res.*, **226**, 49-95, https://doi.org/10.1016/j.atmosres.2019.04.010.

Kubota, T., S. Shige, H. Hashizume, K. Aonashi, N. Takahashi, S. Seto, M. Hirose, Y.N. Takayabu, T. Ushio, K. Nakagawa., K. Iwanami, M. Kachi and K. Okamoto, 2007: Global Precipitation Map Using Satellite-Borne Microwave Radiometers by the GSMaP Project: Production and Validation. *IEEE Trans Geosci Remote Sens*. **45**(7), 2259-2275, https://doi.org/10.1109/TGRS.2007.895337

Kubota, T., T. Iguchi, M. Kojima, L. Liao, T. Masaki, H. Hanado, R. Meneghini, and R. Oki, 2016: A Statistical Method for Reducing Sidelobe Clutter for the Ku-Band Precipitation Radar on board the GPM Core Observatory, *J. Atmos. Oceanic Technol.*, **33**(7), 1413-1428.

Kummerow, C. D., D. L. Randel, M. Kulie, N. Wang, R. Ferraro, S. Joseph Munchak, and V. Petkovic, 2015: The Evolution of the Goddard Profiling Algorithm to a Fully Parametric Scheme. *J. Atmos. Oceanic Technol.*, **32**, 2265–2280, https://doi.org/10.1175/JTECH-D-15-0039.1.

Le, M., V. Chandrasekar, and S. Biswas, 2016: Evaluation and Validation of GPM Dual-Frequency Classification Module after Launch, *J. Atmos. Oceanic Technol*, **33**(12), 2699-2716.

Accepted for publication in *Bulletin of the American Meteorological Society.* DOI 10.1175/BAMS-D-22-0127.1.

Li, Z., M. Chen, S. Gao, Z. Hong, G. Tang, Y. Wen, J.J. Gourley and Y. Hong, 2020: Cross-Examination of Similarity, Difference and Deficiency of Gauge, Radar and Satellite Precipitation Measuring Uncertainties for Extreme Events Using Conventional Metrics and Multiplicative Triple Collocation. *Remote Sens.*, **12**, 1258.

Li, Z., and Coauthors, 2021: Two-decades of GPM IMERG Early and Final Run Products Intercomparison:Similarity and Difference in Climatology, Rates, and Extremes, *J. Hydrol.*, **594**, 125975, https://doi.org/10.1016/j.jhydrol.2021.125975

Li, Z., G. Tang, P. Kirstetter, S. Gao, J.F. Li, Y. Wen and Y. Hong, 2022: Evaluation of GPM IMERG and its constellations in extreme events over the conterminous United States, *J. Hydrol.*, **606**, 127357, https://doi.org/10.1016/j.jhydrol.2021.127357

Liao, L., R. Meneghini, T. Iguchi and A. Detwiler, 2005: Use of Dual-Wavelength Radar for Snow Parameter Estimates, *J. Atmos. Oceanic Technol*, **22**(10), 1494-1506.

Liao, L., and R. Meneghini, 2009: Validation of TRMM precipitation radar through comparison of its multiyear measurements with ground-based radar. *J. Appl. Meteor. Climatol.*, **48**, 804–817.

Liao, L., and R. Meneghini, 2011: A Study on the Feasibility of Dual-Wavelength Radar for Identification of Hydrometeor Phases, J. Appl. Meteor. Climatol., **50**(2), 449-456.

Liao, L. and R. Meneghini, 2022: GPM DPR Retrievals: Algorithm, Evaluation, and Validation. *Remote Sens.*, **14**, 843, https://doi.org/10.3390/rs14040843

Masaki, T. and Coauthors, 2015: Current status of GPM/DPR level 1 algorithm development and DPR calibration, *IEEE International Geoscience and Remote Sensing Symposium*, 2015, pp. 2615-2618, https://doi.org/10.1109/IGARSS.2015.7326348.

Matsui, T., T. Iguchi, X. Li, M. Han, W. Tao, W. Petersen, T. L'Ecuyer, R. Meneghini, W. Olson, C.D. Kummerow, A.Y. Hou, M.R. Schwaller, E.F. Stocker, and J. Kwiatkowski, 2013: GPM Satellite Simulator over Ground Validation Sites, *Bull. Amer. Meteor. Soc.*, **94**(11), 1653-1660

Masaki, T., T. Iguchi, K. Kanemaru, K. Furukawa, N. Yoshida, T. Kubota, and R. Oki, 2020: Calibration of the Dual-frequency Precipitation Radar Onboard the Global Precipitation Measurement Core Observatory. *IEEE Trans. Geosci. Remote Sens.*, **60**, 1-16, https://doi.org/10.1109/TGRS.2020.3039978.

Accepted for publication in *Bulletin of the American Meteorological Society.* DOI 10.1175/BAMS-D-22-0127.1.

Meneghini, R., Kim, H., Liao, L., Kwiatkowski, J., Iguchi, T., 2021: Path attenuation estimates for the GPM Dual-frequency Precipitation Radar. *J. Meteorol. Soc. Japan.*, **99**, 181-200, https://doi.org/10.2151/jmsj.2021-010

Morris, K.R. and M. R. Schwaller, 2010: Data visualization and analysis tools for the Global Precipitation Measurement (GPM) Validation Network, 2010 *IEEE International Geoscience and Remote Sensing Symposium*, pp. 847-850, https://doi.org/10.1109/IGARSS.2010.5654248.

Nakamura, K., 2021: Progress from TRMM to GPM, *J. Meteorol. Soc. Japan*, 99, 3, 697-729

Oki R., T. Iguchi and K. Nakamura, 2020: The GPM DPR Validation Program. *Satellite Precipitation Measurement. Advances in Global Change Research*, V. Levizzani, C. Kidd, D.B. Kirschbaum, C.D. Kummerow, K. Nakamura, F.J. Turk, Ed., *Springer*, 503-514, https://doi.org/10.1007/978-3-030-35798-6_3

Park, H. S., A.V. Ryzhkov, D.S. Zrnić and K. Kim, 2009: The Hydrometeor Classification Algorithm for the Polarimetric WSR-88D: Description and Application to an MCS, *Wea. Forecasting*, **24**(3), 730-748

Protat, A., Louf, V., Soderholm, J., Brook, J., and Ponsonby, W., 2022: Three-way calibration checks using ground-based, ship-based, and spaceborne radars, *Atmos. Meas. Tech.*, 15, 915–926, https://doi.org/10.5194/amt-15-915-2022.

Ryzhkov, A. V. and D. S. Zrnic, 1998: Discrimination between rain and snow with a polarimetric radar. *J. Appl. Meteor.*, **37**, 1228–1240.

Ryzhkov, A. V., S.E. Giangrande, V.M. Melnikov, and T.J. Schuur, 2005: Calibration Issues of Dual-Polarization Radar Measurements, *J. Atmos. Oceanic Technol.*, **22**(8), 1138-1155.

Ryzhkov, A. V., 2007: The Impact of Beam Broadening on the Quality of Radar Polarimetric Data, *J. Atmos. Oceanic Technol.*, **24**(5), 729-744

Schwaller, M. R., and K.R. Morris, 2011: A Ground Validation Network for the Global Precipitation Measurement Mission, *J. Atmos. Oceanic Technol.*, **28**(3), 301-319.

Seto, S., Iguchi, T., & Meneghini, R., 2022: Correction of Path-Integrated Attenuation Estimates Considering the Soil Moisture Effect for the GPM Dual-Frequency Precipitation Radar, *J. Atmos. Oceanic Technol.*, 39(6), 803-821.

Accepted for publication in *Bulletin of the American Meteorological Society.* DOI 10.1175/BAMS-D-22-0127.1.

Skofronick-Jackson, G. and Coauthors, 2017: The Global Precipitation Measurement (Gpm) Mission for Science and Society. *Bull. Am. Meteorol. Soc.* **98**(8), 1679-1695, https://doi.org/10.1175/BAMS-D-15-00306.1

Tang, G., Y. Wen, J. Gao, D. Long, Y. Ma, W. Wan, Y. Hong, 2017: Similarities and differences between three coexisting spaceborne radars in global rainfall and snowfall estimation. *Water Resour. Res.*, **53**(5), 3835-3853.

Toyoshima, K., H. Masunaga, F.A. Furuzawa, 2015: Early Evaluation of Ku- and Ka-Band Sensitivities for the Global Precipitation Measurement (GPM) Dual-Frequency Precipitation Radar (DPR), *SOLA*, **11**, 14-17, https://doi.org/10.2151/sola.2015-004

Warren, R. A., A. Protat, S.T. Siems, H.A. Ramsay, V. Louf, M.J. Manton and T.A. Kane, 2018: Calibrating Ground-Based Radars against TRMM and GPM, *J. Atmos. Oceanic Technol.*, **35**(2), 323-346.

Wang, J., Petersen, W.A., Wolff, D.B. 2021: Validation of Satellite-Based Precipitation Products from TRMM to GPM. Remote Sens., **13**, 1745, https://doi.org/10.3390/rs13091745

Weber, M., and Coauthors, 2021: Towards the Next Generation Operational Meteorological Radar, *Bull. Am. Meteorol. Soc*, **102**(7), E1357-E1383.

Wen, Y., Y. Hong, G. Zhang, T.J. Schuur, J.J., Gourley, Z. Flamig, K.R. Morris, and Q. Cao, 2011: Cross Validation of Spaceborne Radar and Ground Polarimetric Radar Aided by Polarimetric Echo Classification of Hydrometeor Types, *J. Appl. Meteor. Climatol.*, **50**(7), 1389-1402.

Wen, Y., Q. Cao, P.E. Kirstetter, Y. Hong, J.J. Gourley, J. Zhang, G. Zhang, and B. Yong, 2013: Incorporating NASA spaceborne radar data into NOAA National Mosaic QPE system for improved precipitation measurement: a physically based VPR identification and enhancement method. *J. Hydrometeor.*, **14**, 1293– 1307.

Wen, Y., A. Behrangi, B. Lambrigtsen and P.E. Kirstetter, 2016: Evaluation and Uncertainty Estimation of the Latest Radar and Satellite Snowfall Products Using SNOTEL Measurements over Mountainous Regions in Western United States. *Remote Sens.*, **8**. 904, https://doi.org/10.3390/rs8110904.

Accepted for publication in *Bulletin of the American Meteorological Society.* DOI 10.1175/BAMS-D-22-0127.1.

Yin, X., Z. Hu, J. Zheng, B. Li and Y. Zuo, 2021: Study on Radar Echo-Filling in an Occlusion Area by a Deep Learning Algorithm. *Remote Sens*. **13**, 1779, https://doi.org/10.3390/rs13091779

Zhang, G., J. Vivekanandan, and E. A. Brandes, 2001: A method for estimating rain rate and drop size distribution from polarimetric radar, *IEEE Trans. Geosci. Remote Sens.*, **39**, 4, 830– 840.

Zhang, J., K. Howard, C. Langston, B. Kaney, Y. Qi, L. Tang, D. Kitzmiller, 2016: Multi-Radar Multi-Sensor (MRMS) Quantitative Precipitation Estimation: Initial Operating Capabilities. *Bull. Am. Meteorol. Soc.*, **97**(4), 621-638. https://doi.org/10.1175/bams-d-14-00174.1

Accepted for publication in *Bulletin of the American Meteorological Society.* DOI 10.1175/BAMS-D-22-0127.1.